Energy-driven pattern formation

Robert V. Kohn*

Abstract. Many physical systems can be modelled by nonconvex variational problems regularized by higher-order terms. Examples include martensitic phase transformation, micromagnetics, and the Ginzburg–Landau model of nucleation. We are interested in the singular limit, when the coefficient of the higher-order term tends to zero. Our attention is on the internal structure of walls, and the character of microstructure when it forms. We also study the pathways of thermally-activated transitions, modeled via the minimization of action rather than energy. Our viewpoint is variational, focusing on matching upper and lower bounds.

Mathematics Subject Classification (2000). Primary 49-02, 82-02; Secondary 74N15, 82B24, 82D40.

Keywords. Action minimization, Aviles–Giga problem, calculus of variations, cross-tie wall, martensitic transformation, micromagnetics, microstructure.

1. Introduction

Many physical systems are described by nonconvex variational problems regularized by higher-order terms. Two of the simplest examples are the Ginzburg–Landau energy

$$\int_\Omega (u^2-1)^2 + \varepsilon^2 |\nabla u|^2$$

and the Aviles–Giga energy

$$\int_\Omega (|\nabla u|^2-1)^2 + \varepsilon^2 |\nabla\nabla u|^2.$$

The former is a basic model of nucleation; we shall discuss it in Section 4. The latter arises in many settings, including convective pattern formation and magnetic thin films; we shall discuss it in Section 3. Other, more complicated examples include micromagnetics and martensitic transformation; we shall discuss them too, in Section 2. Our focus is always on the singular limit $\varepsilon \to 0$.

In some settings, minimizers get increasingly complicated as $\varepsilon \to 0$. We call this the development of *microstructure*. We shall discuss two examples in Section 2, involving twinning in martensite [40] and the branching of domains in a uniaxial

*This work was partially supported by NSF, most recently through grant DMS0313744.

Proceedings of the International Congress
of Mathematicians, Madrid, Spain, 2006

ferromagnet [13]. When microstructure forms, we are interested in its local character and length scale.

In most settings, minimizers develop sharp transition layers where there is rapid spatial variation. Outside these layers the solution is relatively smooth. We call the transition layers *walls* and the smooth regions *domains*. We are interested in the internal structure of walls, and in evaluating their surface energies. We shall discuss two examples in Section 3, involving the Aviles–Giga energy [38] and cross-tie walls in ferromagnetic thin films [1].

Finally, we are interested in local as well as global minimizers, and in thermally-activated transitions between them. We shall explain in Section 4.1 how large deviation theory leads to the minimization of *action* rather than energy. Then, in Section 4.2, we discuss the singular limit of action minimization for the Ginzburg–Landau functional [42].

Our viewpoint is variational: we focus on the leading-order dependence of the energy upon ε. In problems with microstructure we find the optimal scaling law (Section 2); though the argument does not determine the minimizer, it does give information about its character. In problems involving walls (Sections 3 and 4) the scaling law is obvious and our achievement is to find the prefactor. In the process, we also determine an example of a minimizer.

Upper bounds on the minimum energy are usually easy, by considering appropriate test functions. Lower bounds are much more difficult, however, since our functionals are nonconvex. The main mathematical accomplishment in each of our examples is an ansatz-independent lower bound:

(a) For the examples involving microstructure (Section 2), the heart of the matter is an interpolation inequality (10). It expresses mathematically the fact that development of fine-scale microstructure requires a lot of surface energy.

(b) For the examples involving walls (Section 3), the heart of the matter is the use of a suitable "entropy." Recall that for a conservation law, entropy is dissipated at shocks. Our entropies are analogous, in the sense that the divergence is concentrated at walls.

(c) For the example involving action minimization (Section 4), the heart of the matter is the separation of the action into two parts: the "nucleation cost" and the "propagation cost."

It should be clear by now that our goal is not to survey the field of energy-driven pattern formation. Such a survey would be extremely difficult, because the subject is vast and ill-defined. Even if we limited attention to recent mathematical work based on singularly perturbed variational problems, a survey would have to include diblock-copolymers [11], [55], energy-driven coarsening [41], compressed thin film blisters [7], dislocation patterns in plasticity [17], vortex patterns in type-II superconductors [59], the intermediate state of a type-I superconductor [14], and many

additional examples from micromagnetics [21]. (This list is of course incomplete, and the citations are simply examples selected from a huge literature.)

Our aim is much more limited. The primary goal of this paper is to communicate the methodological developments summarized in (a)–(c) above. In addition, we will explain the materials science problems that led to these developments.

Proving lower bounds is difficult, but guessing them is easier. This is particularly true in problems from physics, where experimental observations are available. Therefore it should not be surprising that many of our results were guessed long ago. For example, the scaling of the minimum energy for a uniaxial ferromagnet (Section 2.2) has been "known" for decades [33], [52]. The cross-tie wall, however, is an exception to this rule. As we shall explain in Section 3.2, the analysis of [1] finds the optimal wall structure explicitly. Prior to that work the structure was known only from numerical and physical experiments [50].

1.1. Warmup: one space dimension. For context and background, it is useful to review a simple 1D example. Consider the minimization of

$$\int_0^1 \frac{1}{\varepsilon}(u_x^2 - 1)^2 + \varepsilon u_{xx}^2 + \alpha u^2 \tag{1}$$

where ε and α are positive. The first term prefers $u_x = \pm 1$; the second penalizes changes of slope; the third penalizes deviations from 0. Their preferences are incompatible, and the competition between them determines the character of the minimizer. When ε is small, the optimal u is a sawtooth function as shown in Figure 1. Its slope is nearly ± 1 except for a transition region (whose length is of order ε) near each peak and valley. The distance between peaks and valleys is determined by the competition

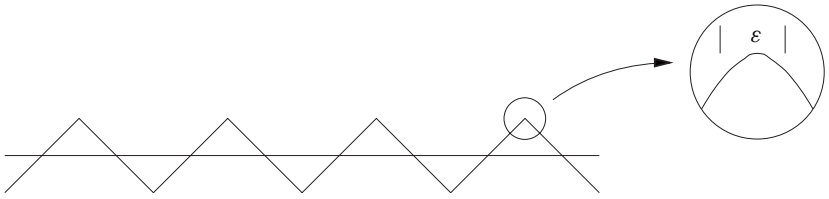

Figure 1. A minimizer of (1).

between the first two terms (which attribute energy to each peak and valley) and the last term (which prefers u to be small). This is most evident in the limit $\varepsilon \to 0$, when each transition layer shrinks to a point. If $2c_0$ is the energy of an (optimal) transition layer, then the limiting variational problem as $\varepsilon \to 0$ is the minimization of

$$\int_0^1 c_0|u_{xx}| + \alpha u^2 \tag{2}$$

subject to the condition $u_x = \pm 1$.

The statement that (2) captures the asymptotic behavior of (1) can be proved with mathematical rigor: this is a basic example of Γ-convergence, see e.g. [9]. In this article we shall work mainly at positive ε, so we do not make use of Γ-convergence in any formal sense. Our viewpoint, however, is very similar. In particular, the following argument – which amounts to the identification of the constant c_0 in (2) [46] – will recur repeatedly. Consider a function u such that $u_x = -1$ near $x = a$ and $u_x = +1$ near $x = b$. Then

$$\int_a^b \frac{1}{\varepsilon}(u_x^2 - 1)^2 + \varepsilon u_{xx}^2 \geq \int_a^b 2|1 - u_x^2||u_{xx}| = \int_a^b |[\Phi(u_x)]_x| \tag{3}$$

if $\Phi'(t) = 2|1 - t^2|$. Since

$$\int_a^b |[\Phi(u_x)]_x| \geq \left| \int_a^b [\Phi(u_x)]_x \right| = |\Phi(1) - \Phi(-1)| = 2\int_{-1}^1 (1 - t^2)$$

we conclude that the cost $2c_0$ of a peak or valley in (1) is at least

$$2\int_{-1}^1 (1 - t^2) = 8/3.$$

Moreover this estimate is sharp, and it reveals the internal character of the transition layer: for equality to hold in (3) we need

$$|1 - u_x^2| = \varepsilon |u_{xx}|$$

from which it follows easily that $u_x = \tanh(x/\varepsilon)$. We have omitted some details, of course; at finite ε the assumptions $u_x(a) = -1$ and $u_x(b) = +1$ are only approximately valid. Still, the preceding calculation captures the heart of the matter.

Our example (1) is local, in the sense that the energy involves only u, u_x, and u_{xx}. But it can also be viewed as a nonlocal problem. Indeed, if we treat $v = u_x$ as our basic variable, and write $u = \nabla^{-1} v$ as an indefinite integral of v, then (1) is equivalent to minimizing

$$\int_0^1 \frac{1}{\varepsilon}(v^2 - 1)^2 + \varepsilon v_x^2 + \alpha |\nabla^{-1} v|^2. \tag{4}$$

From this perspective, space gets divided into "domains" where $v \approx \pm 1$, separated by "walls" where v changes rapidly, on a length scale of order ε.

The problems considered in Sections 2–4 can be viewed as multidimensional analogues of (1) or (4). The multidimensional setting introduces new challenges, and many phenomena not seen in one space dimension. But 1D examples are rich, and their analysis has taught us a lot. For example, these functionals have many local minima, and it is natural to inquire about the character of those states. Are they periodic in x, or can they have "defects"? For studies of this type see [48], [54], [62], [64].

2. Singular perturbation and the development of microstructure

We say a singularly-perturbed variational problem develops microstructure if its minimizers become increasingly complicated as $\varepsilon \to 0$. In this section we discuss two examples, from martensitic transformation and micromagnetics.

2.1. Refinement of twins. A simple 2D analogue of (2) was introduced in 1992 by Kohn and Müller:

$$\min_{\substack{u_y=\pm 1 \\ u=0 \text{ at } x=0}} \int_0^1 \int_0^L u_x^2 + \varepsilon |u_{yy}| \, dx \, dy \tag{5}$$

where $u = u(x, y)$ is scalar-valued. The constraint $u_y = \pm 1$ applies in the interior of the region $(0, L) \times (0, 1)$. It is clearly incompatible with the boundary condition $u = 0$ at $x = 0$, so we expect ∇u to be oscillatory near $x = 0$. The regions where $u_y = \pm 1$ are "domains," and the discontinuities of u_y are "walls." The term $\iint \varepsilon |u_{yy}| \, dx \, dy$ in (5) represents surface energy: since u_y jumps between ± 1 at each interface, it simply counts 2ε times the number of interfaces above x then integrates over $x \in (0, L)$.

This is a simplified model for the geometry of twinning near an austenite twinned-martensite interface, in a crystalline solid undergoing a martensitic phase transformation [39]. Briefly: in the "twinned" region $(0, L) \times (0, 1)$ there are two preferred values $\nabla u = (0, 1)$ and $\nabla u = (0, -1)$, corresponding to two "variants" of martensite. The first term in (5) represents "elastic energy;" it penalizes deviations from the preferred values of ∇u. The second term represents the surface energy of the twin boundaries. We suppose the material occupying the region $x < 0$ is untwinned and rigid; hence the boundary condition $u = 0$ at $x = 0$. See [39] for a more detailed account of the crystallography behind (5), and [8] for a modern introduction to martensitic phase transformation with a variational viewpoint.

The most basic result about (5) is the assertion that

$$C\varepsilon^{2/3} L^{1/3} \leq \text{minimum energy} \leq C' \varepsilon^{2/3} L^{1/3} \tag{6}$$

when ε / L is sufficiently small [40]. Thus, we know the *scaling law* of the minimum energy – though not the prefactor.

The right hand side of (6) – the upper bound – is relatively easy to prove. It suffices to give a single example of a function u with the desired scaling. The convenient construction is self-similar; in particular, the length scale of the twins at x decreases geometrically as x approaches 0. Figure 2a sketches the construction by showing two generations of refinement.

The left hand side of (6) – the lower bound – requires an entirely different type of argument. No example or numerical simulation can be of any use. Rather, we require a geometry-independent argument explaining why no microstructure can do better. In a convex variational problem we would turn to the convex dual. But our example is very nonconvex, due to the constraint $u_y = \pm 1$.

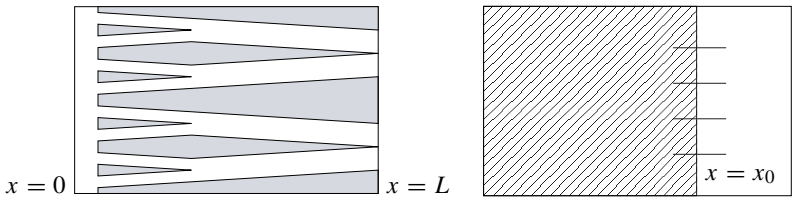

(a) (b)

Figure 2. (a) Two generations of the self-similar construction used to prove the upper bound. (b) Visual aid for the lower bound. If there are few interfaces at x_0 then the integral of u_x^2 over the hatched region must be large.

The successful argument is actually quite elementary. It rests on two simple facts:

Fact 1. *If the graph of f is a sawtooth with few teeth, then it must make large excursions. More precisely: if $f_y = \pm 1$ then*

$$\int_0^1 f^2 \, dy \geq C/(N+1)^2 \quad \textit{if the slope changes } N \textit{ times.}$$

Fact 2. *The integral of u_x^2 controls the variation of u with respect to x. In particular:*

$$\int_0^1 |u(b, y) - u(a, y)|^2 \, dy \leq (b-a) \int_0^1 \int_a^b u_x^2 \, dx \, dy.$$

Using these, the lower bound is proved as follows (c.f. Figure 2b). For any u such that $u = 0$ at $x = 0$ and $u_y = \pm 1$, let

$$E = \int_0^1 \int_0^L u_x^2 + \varepsilon |u_{yy}| \, dx \, dy$$

be the associated energy.

Step 1. Since the second term in E controls the wall energy, for some $0 < x_0 < L$ the number of walls above x_0 is less than or equal a constant times $E/\varepsilon L$. We conclude using Fact 1 that

$$\int_0^1 u^2(x_0, y) \, dy \geq C\varepsilon^2 L^2 / E^2.$$

Step 2. Since the first term in E is u_x^2, the boundary condition together with Fact 2 give

$$LE \geq \int_0^1 u^2(x_0, y) \, dy.$$

Step 3. Combining both steps, we have shown that $LE \geq C\varepsilon^2 L^2/E^2$. Rearrangement gives the desired lower bound $E \geq C\varepsilon^{2/3}L^{1/3}$.

This argument is so easy it leaves one a bit uncomfortable. What makes it work, and how can it be generalized? The answer will become evident in Section 2.2.

In focusing on upper and lower bounds, we have presented only the most basic result concerning (5). Much more can be proved, including an estimate for the length scale of twinning as a function of x [40]. Conti has studied the fine-scale structure of a minimizer near $x = 0$, showing roughly speaking that it is asymptotically self-similar [15].

2.2. Branching of magnetic domains. The branching of domains in a uniaxial ferromagnet combines features of our 1D model problem (1) and our 2D example (5). The problem is richer and more difficult, however, because the domain patterns are fully three-dimensional. A sharp-interface version of this problem was treated in [13]. The following discussion, based on standard micromagnetics and drawn from [21], is only slightly different.

The phenomenon we wish to capture is sketched in Figure 3b; experimental images (which are of course much richer and more detailed) can be found in Section 5.2.1 of [34]. Briefly: we are considering a cylinder occupied by a uniaxial ferromagnet. The magnetization has two preferred values, $m = (1, 0, 0)$ or $m = (-1, 0, 0)$. The observed configurations are local minima of the micromagnetic energy, which is defined by

$$\int_{\text{magnet}} Q(m_2^2 + m_3^2) + \varepsilon^2 |\nabla m|^2 \; + \int_{\text{all space}} |\nabla \phi|^2 \tag{7}$$

where m is the magnetization (a unit vector field defined on the magnet, extended by 0 outside) and ϕ is defined by solving

$$\Delta \phi = \operatorname{div} m. \tag{8}$$

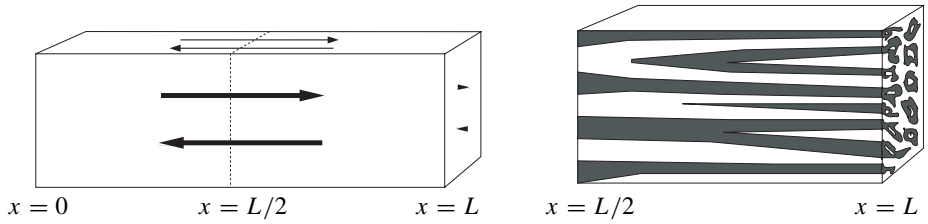

(a) (b)

Figure 3. (a) Sketch of our uniaxial ferromagnet, with the preferred magnetization direction parallel to the axis. (b) Sketch of the magnetic domain structure.

The first term in (7) expresses the anisotropy of the crystal, in other words its preference for $m = (\pm 1, 0, 0)$. The second term, known as the exchange energy, penalizes sharp changes in m and is directly analogous to the term εu_{xx}^2 in our one-dimensional example; when ε is small it forces the creation of walls and determines their energy. The nonlocal magnetostatic energy $\int |\nabla \phi|^2$ comes from Maxwell's equations. It expresses a preference for m to be divergence-free, since (8) is equivalent to the statement that

$$m = \nabla \phi + \text{divergence-free}.$$

(Thus, $\nabla \phi$ is the Helmholtz projection of m onto the space of gradients.)

The origin of the microstructure sketched in Figure 3b is easy to explain heuristically. The magnetization wants to be $(\pm 1, 0, 0)$ in the cylinder, but its extension by 0 to all $\mathbb{R}^3$ wants to be weakly divergence-free. It cannot do both, since being divergence-free would require $m \cdot n$ to vanish at the end of the cylinder. So the magnetization compromises, making the magnetostatic energy small by oscillating rapidly in space between the preferred values $(\pm 1, 0, 0)$ at the end of the cylinder. This requires the introduction of walls across which m_1 changes from 1 to -1. The magnetostatic term likes walls parallel to the x_1-axis (since such walls are weakly divergence-free). However the walls carry surface energy, on account of the exchange term $\varepsilon^2 |\nabla m|^2$. So the domain structure coarsens away from the end of the cylinder – though this means the walls are not exactly parallel to the axis.

Overall: the situation is quite similar to the twinning example discussed in Section 2.1. There ∇u was two-dimensional and exactly curl-free; it developed fine-scale structure near $x = 0$ due to the boundary condition $u = 0$ at $x = 0$. Here m is three-dimensional and only approximately divergence-free; it develops fine-scale structure so that $m \cdot n$ is approximately zero at the end of the cylinder.

Mathematically: the analogue of (6) in this setting is the assertion that for a minimizer,

$$C Q^{1/3} \varepsilon^{2/3} L^{1/3} \leq \frac{\text{energy}}{\text{cross-sectional area}} \leq C' Q^{1/3} \varepsilon^{2/3} L^{1/3} \tag{9}$$

provided Q is sufficiently large and ε / L sufficiently small.

Proving the upper bound is conceptually easy. One must simply give an example of an m with the desired scaling. This is done in [12], [52] for a slightly different model in which interfaces are sharp rather than diffuse. (See see also [21] for a concise summary.) The convenient construction involves branching, but none of the 3D complexity of Figure 3b. Thus the magnetization patterns seen in real magnets are geometrically complicated not because complexity is required for the optimal scaling law, but rather because complexity is a feature of the many local minima consistent with this scaling.

As in Section 2.1, the lower bound provides an entirely different and more interesting challenge. It is natural to simplify the problem slightly by assuming periodicity (rather than a finite-sized magnet) in the x_2 and x_3 variables. This helps by permitting us to focus on the essential physics – namely the competing effects of the anisotropy,

exchange and magnetostatic energies. The main steps are parallel to those of our twinning example:

Fact 0. *The energy controls wall area.*

Fact 1. *Consider a particular section $x_1 = a$. If in this slice the perimeter of the walls is small, then the H^{-1} norm of m_1 must be large.*

Fact 2. *The energy controls the variation of m_1 in the H^{-1} norm.*

Let us explain each assertion briefly. Our twinning example had the wall energy built into the functional, so the analogue of Fact 0 was automatic there. In the present setting we must instead argue as for (3). Since $2xy \le x^2 + y^2$ we have

$$2\varepsilon Q^{1/2}|\nabla m_1| \le \frac{\varepsilon^2}{1-m_1^2}|\nabla m_1|^2 + Q(1-m_1^2).$$

But by differentiating the constraint $m_1^2 + m_2^2 + m_3^2 = 1$ one easily sees that

$$\frac{|\nabla m_1|^2}{1-m_1^2} \le |\nabla m|^2.$$

Therefore

$$2\varepsilon Q^{1/2}\int |\nabla m_1| \le \int Q(m_2^2+m_3^2) + \varepsilon^2|\nabla m|^2.$$

Since $m_1 \approx \pm 1$ in the domains, the left hand side is roughly a constant times the total surface area of the walls. Thus the wall energy is controlled by the sum of anisotropy and exchange energy.

The essence of Fact 1 is the following interpolation inequality: if $S = [0,1]^n$ is the unit cube in $\mathbb{R}^n$ and $g\colon S \to \mathbb{R}$ is periodic with mean value 0 then

$$\int_S g^2 \le C\|g\|_{L^\infty}^{2/3}\left(\int_S |\nabla g|\right)^{2/3}\|g\|_{H^{-1}(S)}^{2/3} \tag{10}$$

where the H^{-1} norm is defined by

$$\|g\|_{H^{-1}(S)}^2 = \int_S |\nabla \Delta^{-1} g|^2$$

Substituting m_1 for g and a scaled section of our cylinder for S, the left hand side of (10) is fixed so the right hand side stipulates a tradeoff between the perimeter $\int |\nabla m_1|$ and the H^{-1} norm of m_1. The interpolation inequality (10) is not exactly standard, but the proof is relatively easy; see e.g. [16] for a concise proof and an interesting extension. Such interpolation inequalities have been used a lot in recent work on energy-driven pattern formation, not only for understanding the consequences of energy minimization, but also for proving bounds on coarsening rates, see e.g. [16], [41], [44]. Their broad importance is due to the special form of the right hand side,

which relates the BV norm (a proxy for perimeter) to a negative norm (a proxy for the length scale of microstructure). Our Fact 1 in Section 2.1 did not assume periodicity; however when f_y is periodic it is an immediate consequence of (10), obtained by taking $S = [0, 1]$ and $g = f_y$.

The essence of Fact 2 is easiest to see in the special case when $\operatorname{div} m = 0$. We also assume m is periodic in x_2 and x_3 with period cell S. Then the variation of m_1 with respect to x_1 is estimated by

$$\|m_1(a,\cdot) - m_1(b,\cdot)\|_{H^{-1}(S)} = \sup_{\int |\nabla v|^2 \le 1} \int_S [m_1(a,\cdot) - m_1(b,\cdot)]v$$

and the right hand side equals

$$\begin{aligned}\int_a^b \int_S (\partial_1 m_1)v &= -\int_a^b \int_S (\partial_2 m_2 + \partial_3 m_3)v \\ &= \int_a^b \int_S (m_2, m_3)\cdot \nabla v \\ &\le \left(\int_a^b \int_S m_2^2 + m_3^2\right)^{1/2} \left(\int_a^b \int_S |\nabla v|^2\right)^{1/2}.\end{aligned}$$

Thus when $\operatorname{div} m = 0$ the variation of m_1 with respect to x_1 in the H^{-1} norm is controlled by the anisotropy energy.

The argument for the lower bound in (9) is parallel to the one sketched in Section 2.1 for (6).

Step 1. If the energy is small then in a generic section the walls have small perimeter (Fact 0). So the H^{-1} norm of m_1 in the section is large (Fact 1).

Step 2. If the energy is small then the H^{-1} norm of m_1 cannot change significantly as x_1 varies (Fact 2). So the H^{-1} norm is large at the end of the cylinder, and (simplifying the argument a bit) this forces the magnetostatic energy to be large.

Step 3. Combining both steps, we find that the energy cannot be small after all.

We have cheated a little. In truth m_1 is neither divergence-free nor exactly mean 0 in each section. The full argument, presented in [13] and [21], proceeds a bit differently, working in Fourier space to take full advantage of the magnetostatic energy. The bottom line, however, is similar to the steps sketched above.

Our understanding of this problem is far less complete than the one discussed in Section 2.1. In particular, while our methods give an estimate for the total area of all the domain boundaries in the magnet, they do not give rigorous results on the local length scale as a function of x.

There are many other problems where nonlocal effects promote microstructure. Bounds analogous to (9) have been proved for a few of them, including diblock

copolymers [11] and the intermediate state of a type-I superconductor [14]. However there are limits to what can be achieved this way. For example, in diblock copolymers the choice of microstructure seems to depend mainly on volume fraction. This cannot be seen from the scaling law; rather, different patterns achieve different prefactors.

3. Singular perturbation and the structure of walls

The problems considered in Section 2 develop microstructure, in the sense that minimizers become increasingly complex as $\varepsilon \to 0$. In proving energy scaling laws, we acquire insight about the character of this microstructure.

Here we turn to a different issue, namely the internal structure of a wall. This question is meaningful and interesting even when there is no microstructure. We begin with a problem of that type – the Aviles–Giga energy – which provides a convenient warmup. Then we discuss the striking recent work of Alouges, Rivière, and Serfaty on the internal structure of a cross-tie wall [1].

3.1. The Aviles–Giga problem. Aviles and Giga asked in [4], [5] what we know about

$$\min_{u=0 \text{ at } \partial\Omega} \int_\Omega \frac{1}{\varepsilon}(|\nabla u|^2 - 1)^2 + \varepsilon |\nabla\nabla u|^2 \tag{11}$$

where Ω is a bounded domain in $\mathbb{R}^2$ and u is a scalar-valued function. Their motivation came from the modeling of smectic liquid crystals, but the same functional arises in the Cross–Newell approach to convective pattern formation [27] and in the modeling of a soft, thin magnetic film with cross-section Ω [38], [63]. Explaining just the last interpretation: the magnetostatic energy prefers $\operatorname{div} m = 0$ in the film and $m \cdot n = 0$ at its edges. If we suppose m depends only on (x, y) then these conditions are equivalent to $(m_1, m_2) = (u_y, -u_x)$ in Ω with $u = 0$ at $\partial\Omega$. The magnetostatic term also prefers $m_3 = \sqrt{1 - |\nabla u|^2}$ to be zero. Thus the sum of magnetostatic and exchange energy is a lot like (11).

As $\varepsilon \to 0$ the energy clearly prefers $|\nabla u| = 1$. If Ω is not a circle then the graph of u must have "folds," and it is natural to guess that if u_ε minimizes (11) then $\lim u_\varepsilon = u_0$ exists and solves a suitable "asymptotic problem" of the form

$$\min_{\substack{|\nabla u|=1 \\ u=0 \text{ at } \partial\Omega}} \int_{\text{folds}} \text{fold energy}. \tag{12}$$

Notice that the class of admissible functions for (12) is somewhat rigid; two examples are shown in Figure 4a.

What is the fold energy? If we assume that the internal structure of a fold is "one-dimensional," i.e. that ∇u depends only on the variable transverse to the fold,

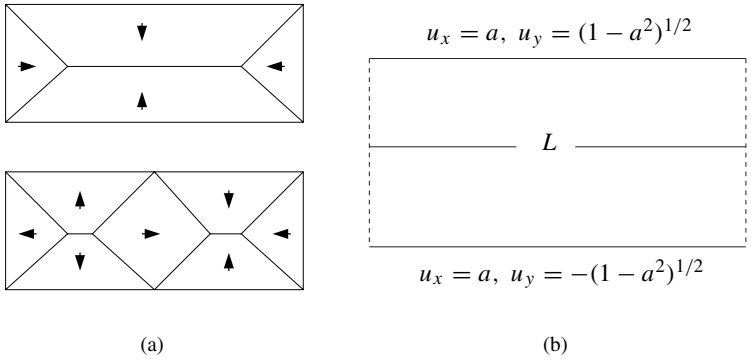

Figure 4. (a) Two admissible configurations for the asymptotic energy (12) (the arrow shows the direction of ∇u). (b) The boundary value problem used to determine the fold energy.

then the energy is easily calculated by an argument similar to (3). The answer is

$$\text{fold energy} = \int_{\text{fold}} \frac{1}{3} \, |[\partial u/\partial n]|^3 \tag{13}$$

where the square bracket denotes the jump of the normal derivative of u across the fold. Thus for a fold parallel to the x-axis across which ∇u jumps from $(a, \sqrt{1-a^2})$ to $(a, -\sqrt{1-a^2})$, the fold energy per unit arc length would be $\frac{8}{3}(1-a^2)^{3/2}$.

But is this calculation right? A proper calculation of the fold energy should assume nothing about its internal structure, proving rather than assuming that it is one dimensional. A scheme for achieving this was introduced in [38]. Focusing for simplicity on folds parallel to the x-axis, the idea is to consider the Aviles–Giga energy in a rectangle, with boundary conditions consistent with a fold as shown in Figure 4b. The height of the strip is 1; the length is L; and ∇u is assumed to be periodic in x with period L. If we can show for such u that

$$\liminf_{\varepsilon \to 0} \int \frac{1}{\varepsilon}(|\nabla u|^2 - 1)^2 + \varepsilon |\nabla \nabla u|^2 \geq \frac{8}{3}(1-a^2)^{3/2} L \tag{14}$$

we will effectively have shown that folds are indeed one-dimensional – or more precisely that there is no incentive to be otherwise.

The proof of (14) involves little more than a clever integration by parts. Suppose we can find a smooth $\Sigma : \mathbb{R}^2 \to \mathbb{R}^2$ such that

$$|\text{div}\, \Sigma(\nabla u)| \leq \frac{1}{\varepsilon}(|\nabla u|^2 - 1)^2 + \varepsilon |\nabla \nabla u|^2 \tag{15}$$

for any $u(x, y)$, with the further property that

$$\Sigma(a, \sqrt{1-a^2}) \cdot (0, 1) + \Sigma(a, -\sqrt{1-a^2}) \cdot (0, -1) = \frac{8}{3}(1-a^2)^{3/2}. \tag{16}$$

Then the integral of the Aviles–Giga energy is bounded below by

$$\int |\text{div } \Sigma(\nabla u)| \geq \left| \int \text{div } \Sigma(\nabla u) \right| = \frac{8}{3}(1-a^2)^{3/2}L \tag{17}$$

using the boundary conditions and periodicity in the last step. This is the desired inequality.

The convenient choice of Σ is

$$\Sigma(\nabla u) = 2\Big(-\frac{1}{3}u_x^3 - u_x u_y^2 + u_x, \frac{1}{3}u_y^3 + u_y u_x^2 - u_y \Big).$$

It satisfies (16), and almost satisfies (15) – there is an extra term on the right hand side, whose value after integration is a constant times ε. Thus the extra term does not matter in the limit $\varepsilon \to 0$, and our argument shows that a one-dimensional wall is asymptotically optimal.

We call Σ an *entropy*. To explain why, notice that if Σ satisfies (15), then (by letting $\varepsilon \to 0$) $\Sigma(\nabla u)$ must be divergence-free wherever u is smooth and $|\nabla u| = 1$. Thus Σ bears the same relation to the eikonal equation that an entropy entropy-flux pair bears to a conservation law.

Our argument shows that a one-dimensional wall is optimal, but it does not show the wall *has* to be one-dimensional. In fact it does not: when $a = 0$ the optimal fold energy is also achieved as $\varepsilon \to 0$ by a two-dimensional pattern similar to a cross-tie wall [60].

We have focused rather narrowly, on the identification of the fold energy, but much more is known. In writing (12) we implicitly assumed that ∇u_ε remains compact, so $|\nabla u_0| = 1$ in the limit; this is true, but the proof is far from trivial [2], [19]. The introduction of entropies and the analogy with conservation laws has led to a lot of progress on this and related problems, including [3], [6], [18], [36], [37], [38], [45], [56], [57]. But the subject is far from finished. In particular, (12) has not yet been shown to be the Γ-limit of (11) as $\varepsilon \to 0$.

3.2. Cross-tie walls. The cross-tie wall is a specific type of domain wall seen in ferromagnetic thin films. Its striking feature is that the cross-tie wall is *not* one dimensional; rather, its structure varies along the wall as well as across it. Its pattern is certainly energy-driven: numerical minimization of the micromagnetic energy produces results quite similar to those seen in real materials. But the simulations do not tell us why the pattern forms or what determines its structure. These questions were recently addressed by Alouges, Rivière, and Serfaty [1]. Our summary will be a bit different from their exposition, following instead the discussion in [21].

As in Section 2.2, our starting point is the micromagnetic energy

$$E = \int_{\text{film}} Q(m_2^2 + m_3^2) + \varepsilon^2 |\nabla m|^2 \; + \int_{\text{all space}} |\nabla \phi|^2$$

where $|m| = 1$ in the film, $m = 0$ outside, and

$$\Delta\phi = \operatorname{div} m.$$

However we are now interested in a soft thin film. The term "soft" means Q is small; in fact we shall take $Q = 0$. The film thickness t should be small, but not too small; when the material is permalloy, cross-tie walls are seen for thicknesses of order 30–80 nm. The model developed in [1] assumes the magnetization m depends only on (x_1, x_2); this is not required energetically [51], but it seems to be a good approximation for a cross-tie wall.

A cross-tie wall can have any angle greater than 90 degrees. To be specific, however, we focus on the case of a 180-degree wall. Its structure is sketched in Figure 5b. This is the magnetization, seen from the top of the film and zooming in on the wall. Far from the wall $(m_1, m_2) = (0, 1)$ at one extreme and $(0, -1)$ at the other. Within the wall m is piecewise smooth and weakly divergence-free. At the discontinuities (which are themselves walls) the angle changes by 90 degrees or less. Experimental images and numerical simulations very much like the figure can be found in [50] (see also [34]).

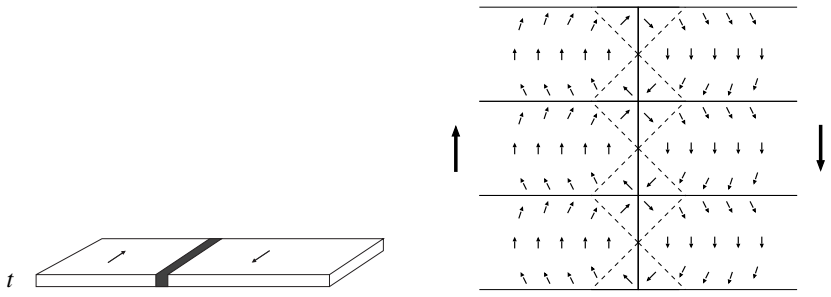

(a) (b)

Figure 5. (a) A thin film with a cross-tie wall, viewed from afar. (b) Magnetization within a 180-degree cross-tie wall, viewed from above the film. In each of the squares along the axis m is piecewise constant; outside those squares the lines of magnetization form circles. The solid vertical and horizontal lines are 1D Néel walls. The dashed lines mark places where m is continuous but not C^1; they are not walls.

The cross-tie wall forms because one-dimensional walls are very expensive when the wall angle is large. The structure shown in Figure 5b consists, in essence, of an ensemble of one-dimensional low-angle walls, whose total energy is less than that of a one-dimensional 180-degree wall.

The preceding intuition is old. It suffices to explain why one should not see large-angle one-dimensional walls. But it does not explain why the specific pattern shown in Figure 5b is optimal. Mathematically: the structure in the figure gives an upper

bound on the wall energy. To know it is optimal we need a matching lower bound. Its proof has three main steps:

Step 1. Simplification of the nonlocal term.

Step 2. Evaluation of the energy of a one-dimensional wall.

Step 3. Use of an appropriate entropy to show the cross-tie pattern is optimal.

We summarize each in turn.

Step 1. The hypothesis that m depends only on (x_1, x_2) makes it easy to evaluate the magnetostatic energy $\int |\nabla\phi|^2$ in terms of the Fourier transform of m. If we assume the relevant spatial frequencies ξ satisfy $t|\xi| \gg 1$ then the expression simplifies and

$$\begin{aligned}\int_{\mathbb{R}^3} |\nabla\phi|^2\,dx &\approx t\int_{\mathbb{R}^2} \frac{|\xi\cdot\hat{m}'|^2}{|\xi|^2}\,d\xi + \int_{\mathbb{R}^2}\frac{|\hat{m}_3|^2}{|\xi|}\,d\xi \\ &= t\|\operatorname{div} m'\|^2_{H^{-1}} + \|m_3\|^2_{H^{-1/2}}\end{aligned} \tag{18}$$

with the convention $m = (m_1, m_2, m_3) = (m', m_3)$. In assuming $t|\xi| \gg 1$ we are not assuming that t is large compared to the width of the cross-tie wall; rather, we are assuming that it is large compared to the width of the low-angle one-dimensional walls inside it. In practice this means $t/\varepsilon \gg 1$. For permalloy the value of ε is 5–10 nm and cross-tie walls are seen when the thickness t is 30–80 nm. Therefore the simplification leading to (18) is plausible, if not entirely compelling.

Step 2. The analysis of a one-dimensional wall in this regime is classical (it is sometimes called a "thick-film Néel wall"). Since the term involving m_3 in (18) has no factor of t, nonzero m_3 is very expensive. Therefore it is natural to assume that $m_3 = 0$. Suppose the wall is perpendicular to the x-axis, with $m = (\cos\theta_\infty, \sin\theta_\infty, 0)$ at one extreme and $m = (\cos\theta_\infty, -\sin\theta_\infty, 0)$ at the other. If the wall profile is $m = (\cos\theta(x), \sin\theta(x), 0)$ then its energy per unit length is

$$\begin{aligned}\int_{\text{film}} \varepsilon^2|\nabla m|^2 + \int_{\text{space}} |\nabla\phi|^2 &= t\int \varepsilon^2|\theta_x|^2\,dx + t\|m_{1x}\|^2_{H^{-1}} \\ &= t\int \varepsilon^2|\theta_x|^2 + |\cos\theta - \cos\theta_\infty|^2\,dx.\end{aligned} \tag{19}$$

This is a one-dimensional variational problem, similar to (1). Solving it, one finds

$$\text{energy density of a 1D wall} = 4\varepsilon t(\sin\theta_\infty - \theta_\infty\cos\theta_\infty). \tag{20}$$

Step 3. It is easy to see that the pattern sketched in Figure 5b does better than a one-dimensional 180-degree wall. Indeed, using (20) and doing some elementary integrations one finds that the figure achieves energy per unit length

$$4\varepsilon t(\sqrt{2} - 1). \tag{21}$$

This beats $4\varepsilon t\big(\sin\frac{\pi}{2} - \frac{\pi}{2}\cos\frac{\pi}{2}\big) = 4\varepsilon t$, the energy of the one-dimensional wall.

But why is the figure optimal? Proceeding as we did for the Aviles–Giga problem, it is natural to consider a rectangle with $(m_1, m_2) = (0, 1)$ on the left, $(m_1, m_2) = (0, -1)$ on the right, and periodic boundary conditions on the top and bottom. Let us focus for simplicity on magnetizations m that are piecewise smooth, with $m_3 = 0$ and $m_1^2 + m_2^2 = 1$, such that $\operatorname{div} m = 0$ weakly (even across any walls). Suppose we can find a differentiable function $\Sigma = [\Sigma_1(m_1, m_2), \Sigma_2(m_1, m_2)]$ such that

$$\operatorname{div} \Sigma(m) = 0 \text{ when } m \text{ is smooth with } \operatorname{div} m = 0 \text{ and } |m| = 1, \tag{22}$$

and such that when m has a weakly divergence-free wall

$$|[\Sigma(m) \cdot n]| \le \text{1D wall energy density}, \tag{23}$$

where $[\Sigma(m) \cdot n]$ is the jump in $\Sigma(m) \cdot n$. Then arguing as in (17), we find that the total energy of the walls in the rectangle is bounded below by the integral of $\Sigma(m) \cdot n$ over the boundary. This shows that

$$\text{energy density of any pattern} \ge \Sigma(0, 1) \cdot (-1, 0) + \Sigma(0, -1) \cdot (1, 0). \tag{24}$$

If in addition to (22) and (23) the right side of (24) is equal to (21) then this argument shows the pattern is optimal within the class under consideration. Remarkably such a Σ exists! The formula is

$$\frac{1}{2\varepsilon t}\Sigma(m) = \begin{cases} \theta m + m^\perp + (0, -\sqrt{2}) & \text{for } -\frac{\pi}{4} \le \theta \le \frac{\pi}{4} \\ \left(\frac{\pi}{2} - \theta\right) m - m^\perp + (-\sqrt{2}, 0) & \text{for } \frac{\pi}{4} \le \theta \le \frac{3\pi}{4} \\ (\theta - \pi) m + m^\perp + (0, \sqrt{2}) & \text{for } \frac{3\pi}{4} \le \theta \le \frac{5\pi}{4} \\ \left(\frac{3\pi}{2} - \theta\right) m - m^\perp + (\sqrt{2}, 0) & \text{for } \frac{5\pi}{4} \le \theta \le \frac{7\pi}{4} \end{cases} \tag{25}$$

when $m = (\cos\theta, \sin\theta)$ and $m^\perp = (-\sin\theta, \cos\theta)$. We emphasize that $\Sigma(m)$ is well-defined for any $m \in S^1$, though θ is only defined modulo 2π. This is important, because there is no reason for θ to be well-defined throughout the rectangle. Rather, the internal walls (where m is discontinuous) can contain vortices – indeed, this is the case for the pattern in Figure 5b.

Why, exactly, does the pattern in the figure achieve equality in the lower bound? The formula (25) specifies Σ separately in four quadrants. One can show that if the internal walls remain in a single quadrant then equality holds in (24). Thus the crucial feature of Figure 5b is that it achieves the effect of a 180-degree wall using only walls with angle 90 degrees or less.

We assumed m was piecewise smooth to capture the main ideas in their simplest possible form. The micromagnetic energy does not permit sharp discontinuities. Therefore the one-dimensional walls in the pattern should be diffuse not sharp; moreover inside such walls we must expect that $\operatorname{div} m \neq 0$, and even (near vortices) that $m_3 \neq 0$. The argument in [1] addresses these subtleties.

It is natural to ask what sets the internal length scale of a cross-tie wall. The answer involves effects we have thus far ignored [20]. Briefly: the anisotropy energy

is small but nonzero; it prefers the length scale to be as small as possible. But at finite t/ε, one-dimensional Néel walls have long tails, which interact repulsively; this favors longer length scales. The internal period of the wall structure is set by the competition between these two effects.

The cross-tie wall is not the only case of a singularly perturbed variational problem whose transition layers are multidimensional. This example is special, however, because we have matching upper and lower bounds – i.e. we know the wall energy, and an optimal wall profile.

4. Action rather than energy minimization

We have been discussing nonconvex variational problems from materials science. Their local minima represent stable states. Since the nonconvexity is extreme, we expect the energy to have multiple minima. We have nevertheless focused on upper and lower bounds rather than on identifying the local minima. This approach is reasonable: in some cases (such as cross-tie walls) nature seems to find the ground state, and in other cases (such as uniaxial ferromagnets) the accessible local minima seem to share many features with the ground state.

But the fact remains: nature finds *local* not global minima. The evidence is all around us. Crystals have defects. Water can be heated above 100 degrees. The bubbles atop a glass of beer appear stable, but they eventually disappear.

These examples reveal more than the mere existence of local minima. They also show that nature escapes from local minima, as a consequence of thermal fluctuation. For a finite-dimensional system with energy $E(z)$, the competition between energy minimization and thermal fluctuation is captured by the stochastic differential equation

$$dz = -\nabla E\, dt + \sqrt{2\gamma}\, dw \tag{26}$$

where w is Brownian motion [32]. If γ is small then the system spends most of its time near the local minima of E. Transitions between the local minima are rare, but they do occur. Their timescales and pathways are predicted by the theory of large deviations [30].

4.1. Action minimization. Suppose $E(z)$ has local minima at z_0 and z_1. The large deviation principle says, roughly speaking, that if a transition from z_0 to z_1 occurs within time T then its pathway is (with very high probability) near the minimizer of the deterministic variational problem

$$S_T = \min_{\substack{z(0)=z_0 \\ z(T)=z_1}} \frac{1}{4} \int_0^T |z_t + \nabla E|^2\, dt. \tag{27}$$

Moreover the transitions are Poisson events, with timescale $e^{-S_T/\gamma}$.

The right hand side of (27) is called the *action*. It amounts in this example to the integrated "equation error" of the deterministic dynamics $z_t = -\nabla E$.

In the limit $T \to \infty$ the action-minimizing path is easy to describe: it goes directly uphill to the lowest mountain pass (saddle point) between z_0 and z_1, then proceeds directly downhill from there. The optimality of this choice is a consequence of the elementary relation

$$\frac{1}{4}\int_0^\tau |z_t + \nabla E|^2\,dt = \frac{1}{4}\int_0^\tau |z_t - \nabla E|^2\,dt + \int_0^\tau \langle z_t, \nabla E\rangle\,dt. \tag{28}$$

The first term is nonnegative, and the second term is $E(z(\tau)) - E(z_0)$. Let τ be the time when the trajectory crosses the ridge between z_0 and z_1. Then the right-hand side of (28) is minimized by the path for which the first term vanishes and $z(\tau)$ is the saddle point. Thus the action-minimizing path goes through the saddle, and the minimal action is the height of the mountain pass. This calculation explains why many studies of phase transition and nucleation reduce to the analysis of saddle points, viewed as "critical nuclei."

Saddle points are only relevant in the limit $T \to \infty$. Indeed, our argument suggested that $\int_0^\tau |z_t - \nabla E|^2\,dt$ should vanish for the optimal trajectory. But climbing from z_0 to the saddle along the steepest-ascent trajectory $z_t = \nabla E$ takes an infinite amount of time. So our calculation is only valid in the limit of large transition times.

Transitions occurring at shorter times T need not go through saddle points, but they are still interesting. This may seem counterintuitive, since such transitions are atypical and extremely rare (the minimum action S_T is a decreasing function of T). But rare, atypical events are often the ones we care about most. For example, suppose the typical lifespan of the hard disk in a computer is 10 years – longer than the lifespan of the machine itself. Then failures within the first year are rare and atypical – but hardly unimportant.

4.2. Ginzburg–Landau. What about infinite dimensional energy-driven systems, like those considered in Sections 2 and 3? Can we understand the character of action-minimizing pathways in the limit $\varepsilon \to 0$? For problems with the complexity of micromagnetics or martensitic phase transformation this question remains open. However for the simpler case of a scalar Ginzburg–Landau model there has been some progress [42], [43].

The Ginzburg–Landau functional is

$$E = \int_\Omega \frac{1}{4\varepsilon}(u^2-1)^2 + \frac{\varepsilon}{2}|\nabla u|^2 \tag{29}$$

where u is scalar valued. In one space dimension this is essentially our warmup problem (4) with $\alpha = 0$. In higher dimensions it is sometimes called the Modica-Mortola functional, and its Γ-limit as $\varepsilon \to 0$ is a constant times the perimeter of the interface separating the two "phases" $u = 1$ and $u = -1$ [46]. The associated

steepest-descent PDE $\dot{u} = -\nabla E$ is known as the Allen–Cahn equation. Its natural timescale (in dimension $n \geq 2$) is $1/\varepsilon$. Rescaling time so the dynamics proceeds with velocity of order 1, i.e. taking $\dot{u} = \varepsilon u_t$, the evolution becomes

$$\varepsilon u_t = \varepsilon \Delta u - \frac{1}{\varepsilon}(u^3 - u). \tag{30}$$

We can write this as $\varepsilon^{1/2} u_t = -\varepsilon^{-1/2} \nabla E$. If Ω is bounded and convex then $u \equiv +1$ and $u \equiv -1$ are the only stable local minima of E [10].

The modeling of thermal fluctuation in this setting is a bit subtle. The analogue of (26) is a stochastic partial differential equation obtained by adding noise to the right hand side of (30). There is no problem if the noise is smooth enough in space. But for modeling thermal fluctuation the noise should be white in space as well as time. The interpretation of such stochastic PDE's and the development of an associated large deviation theory is only complete in space dimension one [28], [31].

Never mind. Action minimization is a deterministic variational problem. It is known to give the pathways and timescales of thermally-activated transitions for the Ginzburg–Landau energy (29) when Ω is one-dimensional. And it seems likely that the same is true when Ω is multidimensional.

Thus we are interested in the minimization of $\int_0^T \int_\Omega |\varepsilon^{1/2} u_t + \varepsilon^{-1/2} \nabla E|^2 \, dx \, dt$. With less shorthand: we are interested in the limiting behavior of

$$\min_{\substack{u \equiv -1 \text{ at } t=0 \\ u \equiv +1 \text{ at } t=T}} \frac{1}{4} \int_0^T \int_\Omega \left| \varepsilon^{1/2} u_t - \varepsilon^{-1/2} (\varepsilon \Delta u - \varepsilon^{-1} (u^3 - u)) \right|^2 dx \, dt \tag{31}$$

as $\varepsilon \to 0$. For simplicity we focus on the case when the domain Ω is a cube in $\mathbb{R}^n$ with periodic boundary conditions.

In one space dimension the answer was found numerically and formally in [24] (see also [29]) and proved in [43]. The optimal pathway is shown schematically in Figure 6. Starting from $u = -1$, it begins by nucleating N equispaced seeds of the $u = 1$ phase (creating $2N$ interfaces). The seeds then grow at constant velocity,

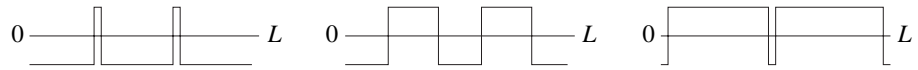

Figure 6. The action-minimizing path for $1D$ Ginzburg–Landau, if the optimal number of seeds is $N = 2$. The configuration is shown at $t = \delta$, $t = T/2$, and $t = T - \delta$.

colliding at exactly time T, leaving the entire interval filled with the $u = 1$ phase. The associated action is

$$\min_{N \geq 1} \left\{ 2N c_0 + \frac{L^2}{9NTc_0} \right\} \tag{32}$$

where N is the number of seeds, $c_0 = 2\sqrt{2}/3$ is the energy of an interface, and L is the length of the interval. The first term in (32) is the cost of nucleating $2N$ interfaces; the second is the cost of their constant-velocity motion.

In two space dimensions the problem has been studied numerically in [24] and analytically in [42], but a complete analysis is still lacking. The anticipated answer is similar to the one-dimensional case, except that (i) if the seeds are points rather than lines then their nucleation cost is negligible; and (ii) if a boundary moves via motion by mean curvature then its propagation cost is negligible. The analogue of (32) is thus

$$\min_{\text{pathways}} \left[(\text{nucleation cost, if any}) + \int_0^T \int (v_{\text{nor}} + \kappa)^2 \right]$$

where v_{nor} is the normal velocity of the moving phase boundary and κ is its curvature. A candidate pathway involving two seeds is shown in Figure 7.

Figure 7. A candidate pathway for $2D$ Ginzburg–Landau, if the optimal number of seeds is $N = 2$. The configuration is shown at $t = \delta$, $t = T/2$, and $t = T - \delta$.

To give a flavor of the analysis, we show under two simplifying assumptions that in one space dimension (with periodic boundary conditions) the action can be no smaller than (32).

Assumption 1. *All interfaces are created at* $t = 0$ *and all annihilations occur at* $t = T$.

Assumption 2. *The energy is "equipartitioned," i.e.*

$$\int_0^L \frac{\varepsilon}{2} u_x^2 \, dx = \int_0^L \frac{1}{4\varepsilon} (u^2 - 1)^2 \, dx = \frac{1}{2} E$$

at each time $0 < t < T$.

If one accepts these, the argument is elementary:

Step 1. If N nuclei form at time 0 (creating $2N$ interfaces), then an application of (28) with $\tau = \delta > 0$ gives

$$\frac{1}{4} \int_0^\delta \int_0^L \left| \varepsilon^{1/2} u_t + \varepsilon^{-1/2} \nabla E \right|^2 \, dx \, dt \geq E(\delta) - E(0) \geq 2N c_0.$$

This accounts for the first term in (32) (the "nucleation cost"). In the rest of argument, we shall show that the remaining action

$$\frac{1}{4} \int_\delta^{T-\delta} \int_0^L \left| \varepsilon^{1/2} u_t + \varepsilon^{-1/2} \nabla E \right|^2 \, dx \, dt$$

is bounded below by the second term in (32) (the "propagation cost").

Step 2. Since no interfaces are created or annihilated at intermediate times (Assumption 2), we have

$$\frac{1}{4}\int_\delta^{T-\delta}\int_0^L \varepsilon u_t^2\,dx\,dt \le \frac{1}{4}\int_\delta^{T-\delta}\int_0^L \varepsilon u_t^2 + \varepsilon^{-1}|\nabla E|^2\,dx\,dt$$
$$= \frac{1}{4}\int_\delta^{T-\delta}\int_0^L \left|\varepsilon^{1/2}u_t + \varepsilon^{-1/2}\nabla E\right|^2\,dx\,dt.$$

Step 3. If N nuclei form (creating $2N$ interfaces), then from Assumptions 1 and 2 we get

$$\int_\delta^{T-\delta}\int_0^L \varepsilon^{-1}(1-u^2)^2\,dx\,dt = \int_\delta^{T-\delta} 2E\,dt = 4c_0N(T-2\delta).$$

where c_0 is the energy of a wall.

Step 4. Using the end conditions $u \equiv -1$ at $t = 0$ and $u \equiv 1$ at $t = T$ we get

$$\int_\delta^{T-\delta}\int_0^L u_t(1-u^2)\,dx\,dt = \frac{4}{3}L + o(1)$$

where $o(1)$ indicates a term tending to 0 with δ. Now,

$$\int_\delta^{T-\delta}\int_0^L u_t(1-u^2)\,dx\,dt \le \left(\int_\delta^{T-\delta}\int_0^L \varepsilon u_t^2\right)^{1/2}\left(\int_\delta^{T-\delta}\int_0^L \varepsilon^{-1}(1-u^2)^2\right)^{1/2}.$$

Step 5. Combining Steps 2, 3, and 4, we find that

$$\liminf_{\delta\to 0}\frac{1}{4}\int_\delta^{T-\delta}\int_0^L \left|\varepsilon^{1/2}u_t + \varepsilon^{-1/2}\nabla E\right|^2 \ge \frac{1}{4}\frac{(4L/3)^2}{4c_0NT} = \frac{L^2}{9c_0NT}.$$

This is the desired bound on the propagation cost.

The rigorous proof in [43] is a bit different. It does not start by demonstrating our two assumptions; rather, their validity becomes clear in the course of the argument. Interestingly, the analysis shares many elements with work on the $\varepsilon \to 0$ limit of the Allen–Cahn equation [35], [61]. The multidimensional problem is also closely related to a conjecture of DeGiorgi concerning the sharp-interface limits of variational problems like

$$\int_\Omega |\nabla E|^2\,dx = \int_\Omega \left|\varepsilon\Delta u - \frac{1}{\varepsilon}(u^3-u)\right|^2 dx;$$

for recent progress on this topic see [47], [49], [58].

We have focused on the singular limit $\varepsilon \to 0$, but there are many other issues in the analysis of thermally-activated transitions. As $T \to \infty$ the pathways go through

mountain passes (saddle points). Surprisingly, though the "mountain pass lemma" has been used by analysts for decades, methods for finding saddle points and transition pathways numerically in high-dimensional systems have mainly been developed by chemists and physicists rather than mathematicians. This is beginning to change; in particular, the "string method" introduced by E, Ren, and Vanden-Eijnden represents an important algorithmic development [22], [23], [25], [26], [53].

References

[1] Alouges F., Rivière, T., Serfaty, S., Néel and cross-tie wall energies for planar magnetic configurations. *ESAIM Control Optim. Calc. Var.* **8** (2002), 31–68.

[2] Ambrosio, L., De Lellis C., Mantegazza, C., Line energies for gradient vector fields in the plane. *Calc. Var. PDE*, **9** (1999), 327–355.

[3] Ambrosio, L., Lecumberry, M., Rivière, T., A viscosity property of minimizing micromagnetic configurations. *Comm. Pure Appl. Math.* **56** (2003), 681–688.

[4] Aviles, P., Giga, Y., A mathematical problem related to the physical theory of liquid crystal configurations. In *Miniconference on geometry and partial differential equations.* 2 (J. Hutchinson and L. Simon, eds.), Proc. Centre Math. Anal. Austral. Nat. Univ. 12, Australian National University, Centre for Mathematical Analysis, Canberra 1987, 1–16.

[5] Aviles, P., Giga, Y., The distance function and defect energy. *Proc. Roy. Soc. Edinburgh* **126A** (1996), 923–938.

[6] Aviles, P., Giga, Y., On lower semicontinuity of a defect obtained by a singular limit of the Ginzburg–Landau type energy for gradient fields. *Proc. Roy. Soc. Edinburgh* **129A** (1999) 1–17.

[7] Ben Belgacem, H., Conti, S., DeSimone, A., Müller, S., Energy scaling of compressed elastic films – three-dimensional elasticity and reduced theories. *Arch. Rational Mech. Anal.* **164** (2002), 1–37.

[8] Bhattacharya, K., *Microstructure of Martensite: Why it forms and how it gives rise to the shape-memory effect*. Oxford Series on Materials Modelling, Oxford University Press, 2003.

[9] Braides, A., Γ*-Convergence for Beginners*. Oxford University Press, Oxford 2002.

[10] Casten, R. G., Holland, C. J., Instability results for reaction diffusion equations with Neumann boundary conditions. *J. Differential Equations* **27** (1978), 266–273.

[11] Choksi, R., Scaling laws in microphase separation of diblock copolymers. *J. Nonlinear Sci.* **11** (2001), 223–236.

[12] Choksi, R., Kohn, R. V., Bounds on the micromagnetic energy of a uniaxial ferromagnet. *Comm. Pure Appl. Math.* **51** (1998), 259–289.

[13] Choksi, R., Kohn, R. V., Otto, F., Domain branching in uniaxial ferromagnets: a scaling law for the minimum energy. *Comm. Math. Phys.* **201** (1999), 61–79.

[14] Choksi, R., Kohn, R. V., Otto, F., Energy minimization and flux domain structure in the intermediate state of a type-I superconductor. *J. Nonlinear Sci.* **14** (2004), 119–171.

[15] Conti, S., Branched microstructures: scaling and asymptotic self-similarity. *Comm. Pure Appl. Math.* **53** (2000), 1448–1474.

[16] Conti, S., Niethammer, B., Otto, F., Coarsening rates in off-critical mixtures. *SIAM J. Math. Anal.* **37** (2006), 1732–1741.

[17] Conti, S., Theil, F., Single-slip elastoplastic microstructures. *Arch. Rational Mech. Anal.* **178** (2005), 125–148.

[18] DeLellis, C., Otto, F., Structure of entropy solutions to the eikonal equation. *J. Eur. Math. Soc.* **5** (2003), 107–145.

[19] DeSimone, A., Kohn, R. V., Müller, S., Otto, F., A compactness result in the gradient theory of phase transitions. *Proc. Roy. Soc. Edinburgh* **131A** (2001), 833–844.

[20] DeSimone, A., Kohn, R. V., Müller, S., Otto, F., Repulsive interaction of Néel walls, and the internal length scale of the cross–tie wall. *Multiscale Model. Simul.* **1** (2003), 57–104.

[21] DeSimone, A., Kohn, R. V., Müller, S., Otto, F., Recent analytical developments in micromagnetics. In *The Science of Hysteresis II: Physical Modeling, Micromagnetics, and Magnetization Dynamics* (G. Bertotti and I. Mayergoyz, eds.), Elsevier, 2006, 269–381.

[22] E, W., Ren, W., Vanden-Eijnden, E., String method for the study of rare events. *Phys. Rev. B* **66** (2002), 052301.

[23] E, W., Ren, W., Vanden-Eijnden, E., Energy landscape and thermally activated switching of submicron-size ferromagnetic elements. *J. Appl. Phys.* **93** (2003), 2275–2282.

[24] E, W., Ren, W., Vanden-Eijnden, E., Minimum action method for the study of rare events. *Comm. Pure Appl. Math* **57** (2004), 637–656.

[25] E, W., Ren, W., Vanden-Eijnden, E., Finite temperature string method for the study of rare events. *J. Chem. Phys.* **109B** (2005), 6688-6693.

[26] E, W., Ren, W., Vanden-Eijnden, E., Transition pathways in complex systems: Reaction coordinates, isocommittor surfaces, and transition tubes. *Chem. Phys. Lett.* **413** (2005), 242–247.

[27] Ercolani, N., Indik, R., Newell, A. C., Passot, T., The geometry of the phase diffusion equation. *J. Nonlinear Sci.* **10** (2000), 223–274.

[28] Faris, W. G., Jona-Lasinio, G., Large fluctuations for a nonlinear heat equation with noise. *J. Phys. A: Math. Gen.* **15** (1982), 3025–3055.

[29] Fogedby, H. C., Hertz, J., Svane, A., Domain wall propagation and nucleation in a two-level system. *Phys. Rev. E* **70** (2004), 031105.

[30] Freidlin, M. L., Wentzell, A. D., *Random Perturbations of Dynamical Systems*. Second edition, Grundlehren Math. Wiss. 260, Springer-Verlag, New York 1998.

[31] Funaki, T., The scaling limit for a stochastic PDE and the separation of phases. *Probab. Theory Related Fields* **102** (1995), 221–288.

[32] Gardiner, C. W., *Handbook of Stochastic Methods for Physics, Chemistry, and the Natural Sciences*. Third edition, Springer Ser. Synergetics 13, Springer-Verlag, Berlin 2004.

[33] Hubert, A., Zur Theorie der zweiphasigen Domänenstrukturen in Supraleitern und Ferromagneten. *Phys. Stat. Solidi* **24** (1967), 669–682.

[34] Hubert, A., R. Schäfer, R., *Magnetic Domains: The Analysis of Magnetic Microstructures*. Springer-Verlag, 1998.

[35] Hutchinson, J., Tonegawa, Y., Convergence of phase interfaces in the van der Waals-Cahn-Hilliard theory. *Calc. Var. PDE* **10** (2000), 49–84.

[36] Jabin, P. E., Perthame, B., Compactness in Ginzburg-Landau energy by kinetic averaging. *Comm. Pure Appl. Math.* **54** (2001), 1096–1109.

[37] Jabin, P. E., Perthame, B., Otto, F., Line-energy Ginzburg-Landau models: zero-energy states. *Ann. Sc. Norm. Super. Pisa Cl. Sci.* (5) **1** (2002), 187–202.

[38] Jin, W., Kohn, R. V., Singular perturbation and the energy of folds. *J. Nonlinear Sci.* **10** (2000), 355–390.

[39] Kohn, R. V., Müller, S., Branching of twins near an austenite-twinned-martensite interface. *Phil. Mag. A* **66** (1992), 697–715.

[40] Kohn, R. V., Müller, S., Surface energy and microstructure in coherent phase transitions. *Comm. Pure Appl. Math.* **47** (1994), 405–435.

[41] Kohn, R. V., Otto, F., Upper bounds on coarsening rates. *Comm. Math. Phys.* **229** (2002), 375–395.

[42] Kohn, R. V., Otto, F., Reznikoff, M.G., Vanden-Eijnden, E., Action minimization and sharp-interface limits for the stochastic Allen-Cahn equation *Comm. Pure Appl. Math.*, to appear.

[43] Kohn, R. V., Reznikoff, M.G., Tonegawa, Y., The sharp-interface limit of the action functional for Allen-Cahn in one space dimension. *Calc. Var. PDE* **25** (2006), 503–534.

[44] Kohn, R. V., Yan, X., Coarsening rates for models of multicomponent phase separation. *Interfaces and Free Boundaries* **6** (2004) 135–149.

[45] Lecumberry, M., Rivière, T., Regularity for micromagnetic configurations having zero jump energy. *Calc. Var. PDE* **15** (2002) 389–402.

[46] Modica, L., Mortola, S., Un esempio di Γ-convergenza. *Boll. Un. Mat. Ital.* **14** (1977), 285–299.

[47] Moser, R., A higher-order asymptotic problem related to phase transitions. *SIAM J. Math. Anal.* **37** (2005) 712–736.

[48] Müller, S., Singular perturbation as a selection mechanism for periodic minimizing sequences. *Calc. Var. PDE* **1** (1993), 169–204.

[49] Nagase, Y., Tonegawa, Y., A singular perturbation problem with integral curvature bound. Preprint.

[50] Nakatani, Y., Uesaka, Y., Hayashi, N., Direct solution for the Landau-Lifshitz-Gilbert equation for micromagnetics. *Japan J. Appl. Phys.* **28** (1989), 2485–2507.

[51] Otto, F., Cross-over in scaling laws: a simple example from micromagnetics. *Proceedings of the International Congress of Mathematicians* (Beijing, 2002), Vol. III, Higher Ed. Press, Beijing 2002, 829–838.

[52] Privorotskii, I. *Thermodynamics of Domain Structures*. John Wiley & Sons, 1976.

[53] Ren, W., Higher order string method for finding minimum energy paths. *Comm. Math. Sci.* **1** (2003), 377–384.

[54] Ren, X., Truskinovsky, L., Finite scale microstructures in nonlocal elasticity. *J. Elasticity* **59** (2000), 319–355.

[55] Ren, X., Wei, J., On energy minimizers of the diblock copolymer problem. *Interfaces Free Bound.* **5** (2003), 193–238.

[56] Rivière, T., Serfaty, S., Limiting domain wall energy for a problem related to micromagnetics. *Comm. Pure Appl. Math.* **54** (2001), 294–338.

[57] Rivière, T., Serfaty, S., Compactness, kinetic formulation, and entropies for a problem related to micromagnetics, *Comm. Partial Differential Equations* **28** (2003), 249–269.

[58] Röger, M., Schätzle, R., On a modified conjecture of DeGiorgi. Preprint.

[59] Sandier, E., Serfaty, S., *Vortices in the Magnetic Ginzburg–Landau Model*. Progr. Nonlinear Differential Equations Appl. 70, Birkhäuser, Boston 2007, to appear.

[60] Serfaty, S., personal communication.

[61] Tonegawa, Y., Phase field model with a variable chemical potential. *Proc. Roy. Soc. Edinburgh* **132A** (2002), 993–1019.

[62] Truskinovsky, L., Zanzotto, G., Ericksen's bar revisited: energy wiggles. *J. Mech. Phys. Solids* **44** (1996), 1371–1408.

[63] van den Berg, H. A. M. Self–consistent domain theory in soft–ferromagnetic media. II. Basic domain structures in thin film objects. *J. Appl. Phys.* **60** (1986), 1104–1113.

[64] Yip, N. K., Structure of stable solutions of a one-dimensional variational problem. *ESAIM Control Optim. Calc. Var.*, to appear.

Courant Institute, NYU, 251 Mercer Street, New York, NY 10012, U.S.A.
E-mail: kohn@cims.nyu.edu